Improved Optimal Duty Model Predictive Current Control Strategy for PMSM*

Dingdou Wen, *Jie Yuan*, *Yang Zhang** *and Chuandong Shi*
(School of Electrical and Information Engineering,
Hunan University of Technology, Zhuzhou 412007, China)

Abstract: To further improve the steady-state performance of the conventional dual vector model predictive current control (MPCC), an improved optimal duty MPCC strategy for permanent magnet synchronous motor (PMSM) is proposed. This strategy is realized by selecting an optimal voltage vector combination and its duration from the five basic voltage vector combinations, followed by acting on the inverter. The five combinations are: the combination of the optimal voltage vector at the previous moment and basic voltage vector with an angle difference of 60°; the combination of the optimal voltage vector at the previous moment and basic voltage vector with an angle difference of –60°; the combination of the aforementioned three basic voltage vectors with the zero vector. Experimental results indicate that the method effectively reduces the stator current ripple without increasing the calculational burden. Furthermore, it improves the steady-state performance of the system without altering the dynamic performance of the system.

Keywords: Model predictive current control, improved optimal duty, optimal voltage vector combination, steady-state performance, PMSM

1 Introduction

At present, predictive control with current as the control target is divided into two categories: model predictive control (MPC) [1] and deadbeat predictive control (DPC) [2]. The purpose of DPC is to make the control target strictly follow the given target, and then realize deadbeat control. From the control process perspective, the method is simple in principle and easy to implement. However, in terms of improving the control performance of the system, sampling and calculation delays are concerning issues [3]. In addition, this method cannot achieve multi-objective comprehensive optimization as the MPC because it does not involve the design of cost functions. Conversely, MPC is more attractive to scholars owing to its several advantages, such as its simple algorithm and ability to address complex constraint optimization problems of nonlinear systems [4]. MPC can be divided into generalized predictive control (GPC) and finite control set MPC (FCS-MPC) [5]. Because of the robust coupling, nonlinearity, and small electrical constants of a permanent magnet synchronous motor (PMSM), applying generalized MPC directly to AC speed regulation systems remains challenging. Therefore, FCS-MPC has become a hot topic in the field of current motor drive control [6-7].

In addition, the conventional FCS-MPC can only select one of the seven basic voltage vectors as the optimal voltage vector via rolling optimization, thereby degrading the steady-state performance. The improved method proposed in Refs. [8-17] adopts the multi-vector FCS-MPC. The duty cycle model predictive current control (MPCC) method (second voltage vector is fixed to the zero vector.) is used in Refs. [8-11, 17]. This method modulates the basic and zero vectors, and the duration of each voltage vector is calculated by the duty cycle. The output optimal voltage vector amplitude is adjustable, which improves the control performance of the system to a certain extent. To further improve the steady-state performance of the duty cycle MPCC,

Manuscript received February 22, 2021; revised May 23, 2021; accepted June 29, 2021. Date of publication September 30, 2022; date of current version March 7, 2022.
* Corresponding Author, E-mail: hut_zy@163.com
* Supported by the National Natural Science Foundation of China (51907061), Natural Science Foundation of Hunan Province(2019JJ50119) and National Engineering Laboratory of UHV Engineering Technology (Kunming, Guangzhou)(NEL202008).
Digital Object Identifier: 10.23919/CJEE.2022.000032

the method is no longer limited to the combination of the basic and zero vectors, which is proposed in Refs. [12-14]. This method considers that the amplitude and direction of the output optimal voltage vector are adjustable, and the current ripple is significantly reduced. Specifically, a two-vector-based model predictive torque control, without weighting factors for induction motor drives, is proposed in Ref. [12]. This method circumvents the design of weight coefficients and selects the optimal voltage vector combination among 18 different voltage vector combinations. After selecting the first optimal voltage vector in Ref. [13], the optimal voltage vector combination is selected from seven combinations of the first optimal voltage vector and the remaining basic voltage vectors. In Ref. [14], the proposed algorithm adds six virtual voltage vectors and optimizes the finite control set, eventually leading to only five candidate voltage vectors in the system. A combination of two voltage and zero vectors applied in one cycle can be used to improve the steady-state performance of the system. Although it is proposed in Refs. [15-16], this type of algorithm is limited by its complex calculation and difficult implementation.

To improve the steady-state performance of the conventional dual vector MPCC system, without significantly increasing the computational burden of the algorithm, an improved optimal duty MPCC strategy is proposed in this study. After obtaining the position of the optimal voltage vector at the previous moment, the combination of the voltage vector at the next moment was optimized. The five combinations of the candidate voltage vectors at the next moment are as follows: the optimal effective voltage vector at the last moment, and the two vectors with a difference of 60° before and after are combined in pairs, according to the principle of being adjacent; the above three effective vectors are combined with zero vectors. The duration of the voltage vector is calculated by the i_q deadbeat principle, and an optimal voltage vector combination is selected from the five combinations according to the principle of minimizing the cost function. The simulation and experimental results indicate that the improved MPCC can exhibit better steady-state performance in the proposed scheme than the conventional MPCC, although the number of candidate voltage vectors is halved. In addition, in the full speed range, its current ripple value is lower than the conventional MPCC, and its dynamic performance remains unaltered.

2 Discrete mathematical model of PMSM

The current state equation of surface PMSM in synchronous rotating coordinate system is expressed as

$$\frac{\mathrm{d}i_{\mathrm{q}}}{\mathrm{d}t}=\frac{1}{L_{\mathrm{S}}}\left(u_{\mathrm{q}}-R_{\mathrm{S}}i_{\mathrm{q}}-\omega_{\mathrm{e}}L_{\mathrm{S}}i_{\mathrm{d}}-\omega_{\mathrm{e}}\psi_{\mathrm{f}}\right) \tag{1}$$

$$\frac{\mathrm{d}i_{\mathrm{d}}}{\mathrm{d}t}=\frac{1}{L_{\mathrm{s}}}\left(u_{\mathrm{d}}-R_{\mathrm{s}}i_{\mathrm{d}}+\omega_{\mathrm{e}}L_{\mathrm{s}}i_{\mathrm{q}}\right) \tag{2}$$

where u_{d} is the direct axis component of the stator voltage; u_{q} is the quadrature axis component of the stator voltage; i_{d} is the direct axis component of the stator current; i_{q} is the quadrature axis component of the stator current; R_{s} is the stator resistance; L_{s} is the stator inductance; ω_{e} is the rotor electrical velocity; ψ_{f} is the permanent magnet flux linkage.

The current prediction model is obtained via discretization processing of Eqs. (1) and (2).

$$i_{\mathrm{q}}(k+1)=i_{\mathrm{q}}(k)+\frac{T_{\mathrm{S}}}{L_{\mathrm{S}}}\left[u_{\mathrm{q}}(k)-R_{\mathrm{S}}i_{\mathrm{q}}(k)+E_{\mathrm{q}}(k)\right] \tag{3}$$

$$i_{\mathrm{d}}(k+1)=i_{\mathrm{d}}(k)+\frac{T_{\mathrm{s}}}{L_{\mathrm{s}}}\left[u_{\mathrm{d}}(k)-R_{\mathrm{s}}i_{\mathrm{d}}(k)+E_{\mathrm{d}}(k)\right] \tag{4}$$

$$E_{\mathrm{q}}(k)=-\omega_{\mathrm{e}}(k)L_{\mathrm{s}}i_{\mathrm{d}}(k)-\omega_{\mathrm{e}}(k)\psi_{\mathrm{f}} \tag{5}$$

$$E_{\mathrm{d}}(k)=\omega_{\mathrm{e}}(k)L_{\mathrm{s}}i_{\mathrm{q}}(k) \tag{6}$$

where $i_{\mathrm{d}}(k)$, $i_{\mathrm{q}}(k)$, $i_{\mathrm{d}}(k+1)$, and $i_{\mathrm{q}}(k+1)$ represent d- and q-axes state current at the kth and (k+1)th sampling instants, respectively. $E_{\mathrm{d}}(k)$ and $E_{\mathrm{q}}(k)$ represent the values of the orthogonal axis component of the motor back EMF at the current moment. T_{s} is the sampling period. $u_{\mathrm{d}}(k)$ and $u_{\mathrm{q}}(k)$ denote the d- and q-axes state voltage at the kth sampling instant, respectively. $\omega_{\mathrm{e}}(k)$ is the state rotor electrical velocity at the kth sampling instant.

3 Proposed MPCC

3.1 Conventional MPCC strategy with optimal duty cycle

The schematic diagram of the conventional optimal duty cycle control strategy (ODC-MPCC), which selects the voltage vector, is presented in Fig. 1. Notably, the six nonzero voltage vectors have been optimized simultaneously with the duty cycle.

In Fig. 1, $i_q(k+1)$, $i_q(k)$, i_{qref}, and T_s represent the predicted value of the quadrature axis current at the next moment, feedback value of the quadrature axis current at the current moment, given value of the quadrature axis current obtained from the speed outer loop, and sampling period, respectively.

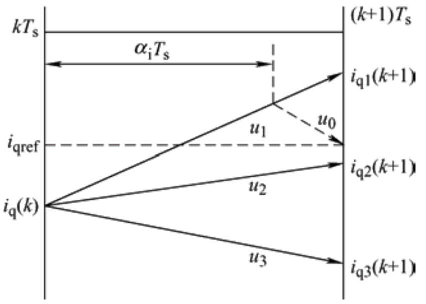

Fig. 1 Schematic diagram of voltage vector selection for ODC-MPCC strategy

The i_q deadbeat principle is expressed as

$$i_q(k+1) = i_q(k) + s_{opt} t_{opt} + s_0 (T_s - t_{opt}) = i_{q\,ref} \tag{7}$$

where t_{opt}, s_{opt}, and s_0 represent the duration of the optimal voltage vector, i_q slope when the optimal voltage vector is applied, and i_q slope when the null voltage vector is applied, respectively.

The duty cycle α_i can be obtained by solving Eq. (7).

$$\alpha_i = \frac{t_{opt}}{T_s} = \frac{i_{qref} - i_q(k) - s_0 T_s}{T_s (s_{opt} - s_0)} \tag{8}$$

$$s_0 = \frac{1}{L_s}\left(-R_s i_q - \omega_e L_s i_d - \omega_e \psi_f\right) \tag{9}$$

$$s_i = s_0 + \frac{u_{qi}}{L_s} \tag{10}$$

where u_{qi} is the stator voltage q-axis component corresponding to the ith voltage vector, i=1, 2, ⋯, 6.

The cost function g_i is used to describe the relationship between the reference current and predicted current, which is expressed as

$$g_i = \left|i_{qref} - i_q(k+1)\right| + \left|i_{dref} - i_d(k+1)\right| \tag{11}$$

The six optimized effective voltage vectors are introduced into Eqs. (3) and (4). The optimal voltage vector is the voltage vector that minimizes the value of g_i.

3.2 Improved MPCC strategy with optimal duty cycle

3.2.1 Selection of voltage vector

ODC-MPCC optimizes the duty cycle and basic voltage vector simultaneously to obtain six virtual voltage vectors. These six virtual voltage vectors are adjustable in size and fixed in direction. To improve the steady-state performance of conventional ODC-MPCC, an improved optimal duty MPCC (IOD-MPCC) is proposed.

In the first sampling period, IOD-MPCC adopts the same method as ODC-MPCC to determine the optimal voltage vector. In other sampling periods, IOD-MPCC performs rapid positioning based on the optimal voltage vector selected at the previous moment. The candidate vectors are limited to three basic voltage vectors, which include the optimal voltage vector at the previous moment and two basic voltage vectors with a phase angle difference of ±π/3 from the optimal voltage vector. The proposed MPCC voltage vector selection table is presented in Tab. 1.

Tab. 1 Proposed MPCC voltage vector selection

Optimal voltage vector at the previous moment	Alternative effective voltage vector at the next moment
$\boldsymbol{u}_1$	$\boldsymbol{u}_1$, $\boldsymbol{u}_2$, $\boldsymbol{u}_6$
$\boldsymbol{u}_2$	$\boldsymbol{u}_2$, $\boldsymbol{u}_3$, $\boldsymbol{u}_1$
$\boldsymbol{u}_3$	$\boldsymbol{u}_3$, $\boldsymbol{u}_2$, $\boldsymbol{u}_4$
$\boldsymbol{u}_4$	$\boldsymbol{u}_4$, $\boldsymbol{u}_3$, $\boldsymbol{u}_5$
$\boldsymbol{u}_5$	$\boldsymbol{u}_5$, $\boldsymbol{u}_4$, $\boldsymbol{u}_6$
$\boldsymbol{u}_6$	$\boldsymbol{u}_6$, $\boldsymbol{u}_5$, $\boldsymbol{u}_1$

To ensure a constant switching frequency, each group of switches is only allowed to jump once during the pulse generation phase. There are five effective combinations among the four voltage vectors, (three nonzero voltage vectors and one zero vector). Assuming that the optimal voltage vector at the last moment is u_1, the five sets of candidate voltage vector combinations of IOD-MPCC are ($\boldsymbol{u}_1$, $\boldsymbol{u}_0$), ($\boldsymbol{u}_2$, $\boldsymbol{u}_0$), ($\boldsymbol{u}_6$, $\boldsymbol{u}_0$), ($\boldsymbol{u}_1$, $\boldsymbol{u}_2$), and ($\boldsymbol{u}_1$, $\boldsymbol{u}_6$).

When assessing the location of the optimal voltage vector at the previous moment, two situations require specific explanations.

(1) As illustrated in Fig. 2a, when the motor speed (N_r) and motor torque (T_e) are changed abruptly, assuming

that the optimal voltage vector at the previous moment is $\boldsymbol{u}_1$, the candidate vectors at the current moment are $\boldsymbol{u}_6$, $\boldsymbol{u}_1$, and $\boldsymbol{u}_2$. However, the reference voltage vector ($\boldsymbol{u}_i$) may be in the third sector. Evidently, the current candidate vectors $\boldsymbol{u}_6$, $\boldsymbol{u}_1$, and $\boldsymbol{u}_2$ are not globally optimal. In this case, the optimal voltage vector must be determined from the six nonzero voltage vectors.

(2) As illustrated in Fig. 2b, if the selected voltage vector combination contains two effective nonzero voltage vectors, the principle for assessing the position of the optimal voltage vector at the previous moment is defined to compare the duration of the two nonzero voltage vectors. For example, the optimal voltage vector combination at the final moment is $\boldsymbol{u}_2$ and $\boldsymbol{u}_1$, the duration of $\boldsymbol{u}_1$ is t_1, and the duration of u_2 is (T_s–t_1). When t_1>T_s /2, the duration of $\boldsymbol{u}_1$ exceeds that of $\boldsymbol{u}_2$, which indicates that the final synthesized voltage vector is closer to $\boldsymbol{u}_1$; hence, the optimal voltage vector location at the next moment should be selected as $\boldsymbol{u}_1$.

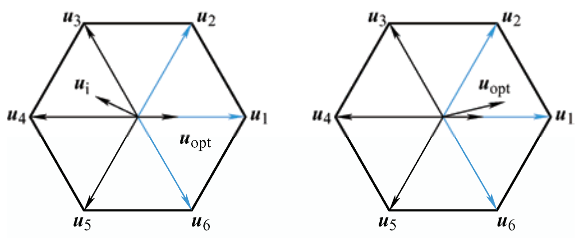

(a) Special cases (b) Normal situation

Fig. 2 Schematic diagram of the optimal voltage vector position under special circumstances

3.2.2 Calculation of voltage vector duration

The duration distribution process of each voltage vector in the five combinations is presented as follows.

The quadrature axis current deadbeat principle is used to calculate the duration of the selected voltage vector u_i, u_j. The corresponding equation is expressed as

$$i_q(k+1)=i_q(k)+s_it_i+s_jt_j=i_q(k)+s_it_i+s_j(T_s-t_i)=i_{qref} \tag{12}$$

where t_i, (T_s–t_i), and s_i, s_j represent the duration of $\boldsymbol{u}_i$, duration of $\boldsymbol{u}_j$, and i_q slopes when $\boldsymbol{u}_i$ and $\boldsymbol{u}_j$ are applied, respectively.

By solving Eq. (12), the duration of the selected voltage vector $\boldsymbol{u}_i$, $\boldsymbol{u}_j$ is obtained as

$$t_i=\frac{i_{qref}-i_q(k)-s_jT_s}{s_i-s_j} \tag{13}$$

$$t_j=T_s-t_i \tag{14}$$

where $s_i=s_0+\frac{u_{qi}}{L_s}$ and $s_j=s_0+\frac{u_{qj}}{L_s}$.

When the system performs rolling optimization, u_d, u_q in Eqs. (3) and (4) are replaced by the following equations

$$u_q=u_{qi}t_i+u_{qj}(T_s-t_i) \tag{15}$$

$$u_d=u_{di}t_i+u_{dj}(T_s-t_i) \tag{16}$$

where u_{qi} and u_{qj} are the q-axis components of the stator voltage corresponding to $\boldsymbol{u}_i$ and $\boldsymbol{u}_j$, respectively. In addition, u_{di} and u_{dj} are the d-axis components of the stator voltage corresponding to $\boldsymbol{u}_i$ and $\boldsymbol{u}_j$ respectively.

3.2.3 Voltage vector analysis

The schematic diagram of the optional voltage vector range of ODC-MPCC and IOD-MPCC is presented in Fig. 3.

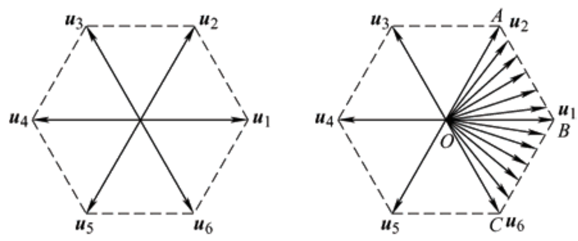

(a) ODC-MPCC (b) IOD-MPCC

Fig. 3 Schematic diagram of selectable voltage vector range for two control methods

When comparing the selectable voltage vector ranges, the optimal voltage vector $\boldsymbol{u}_1$ at the previous moment is used as an example. When ODC-MPCC searches for the optimal voltage vector combination in the next sampling period, the six sets of ODC-MPCC candidate vector combinations are ($\boldsymbol{u}_1$, $\boldsymbol{u}_0$), ($\boldsymbol{u}_2$, $\boldsymbol{u}_0$), ($\boldsymbol{u}_3$, $\boldsymbol{u}_0$), ($\boldsymbol{u}_4$, $\boldsymbol{u}_0$), ($\boldsymbol{u}_5$, $\boldsymbol{u}_0$), and ($\boldsymbol{u}_6$, $\boldsymbol{u}_0$). In this combination, the second voltage vector is fixed as a zero vector. The voltage vector synthesized by ODC-MPCC can only adjust the amplitude of the voltage vector. The optional voltage vector range of ODC-MPCC is illustrated in Fig. 3a. The five sets of IOD-MPCC candidate vector combinations are ($\boldsymbol{u}_1$, $\boldsymbol{u}_0$), ($\boldsymbol{u}_2$, $\boldsymbol{u}_0$), ($\boldsymbol{u}_6$, $\boldsymbol{u}_0$), ($\boldsymbol{u}_1$, $\boldsymbol{u}_2$), and ($\boldsymbol{u}_1$, $\boldsymbol{u}_6$). The voltage vector synthesized by IOD-MPCC has an adjustable amplitude direction. The selectable voltage vector range of IOD-MPCC is shown in Fig. 3b. The combined voltage vector direction is between $\boldsymbol{u}_2$ and $\boldsymbol{u}_6$, and the voltage vector length falls on two sides of the regular hexagon, AB and BC and OB.

The vector ranges for ODC-MPCC and IOD-MPCC are presented in Fig. 3, which depicts that although the limited control set of IOD-MPCC only contains three basic voltage vectors, the range of the optional voltage vector combinations is significantly expanded. Hence, IOD-MPCC exhibits better steady-state performance than ODC-MPCC.

The following steps are required to implement the improved MPCC strategy.

(1) The position of the optimal voltage vector selected at the previous moment is used to determine the positions of the three candidate nonzero voltage vectors at the next moment.

(2) Eq. (13) is used to calculate the duration of the vector to be selected in each combination in five combinations, and five sets of current prediction values are obtained from Eqs. (3) and (4).

(3) Eq. (11) is used to calculate the cost function values corresponding to the five groups of current prediction values, and the optimal voltage vector combination is selected.

(4) The switching state and duration corresponding to the selected voltage vector combination are applied to the inverter.

The block diagram of the proposed MPCC control strategy is presented in Fig. 4.

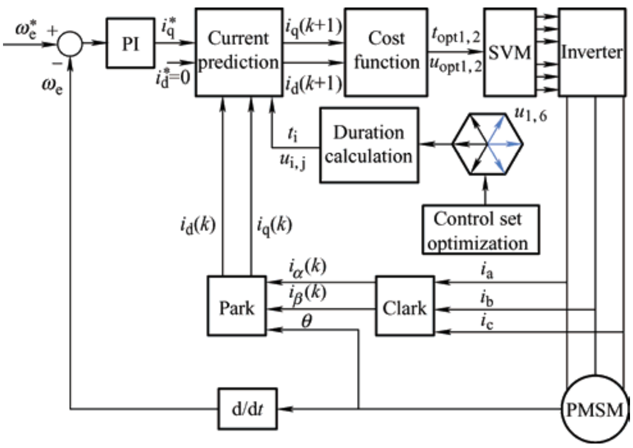

Fig. 4 Control block diagram of the proposed MPCC

4 Analysis of experimental results

To verify the effectiveness and feasibility of the proposed method, two control methods were verified on the RT-LAB platform. The experimental platform is illustrated in Fig. 5. The PMSM parameters are presented in Tab. 2. Here, the sampling frequency is 10 kHz. The experimental waveforms are presented in Figs. 6-9.

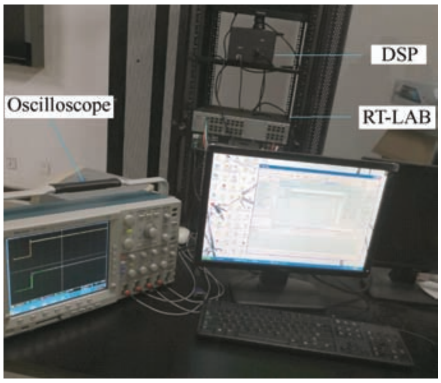

Fig. 5 RT-LAB experiment platform

Tab. 2 PMSM parameters

Parameter	Value
Rotor flux linkage/Wb	0.1
Stator resistance/Ω	0.15
Stator inductance/mH	1.625
Rated torque/(N·m)	15
Rated speed/(r/min)	3 000
Inertia/(kg·m^2)	0.004 78
Pole pairs	4

4.1 Steady state analysis

The A-phase stator current waveform and its total harmonic distortion (THD) analysis diagram of the motor running at a rated torque (15 N·m) and rated speed (3 000 r/min) are presented in Fig. 6. The THD value of the A-phase stator current in the conventional ODC-MPCC algorithm is 10.79%; however, this value is reduced by 20% in the IOD-MPCC algorithm (8.59%). From the experimental results, we conclude that the expansion of the second voltage vector selection range can improve the steady-state performance of the system.

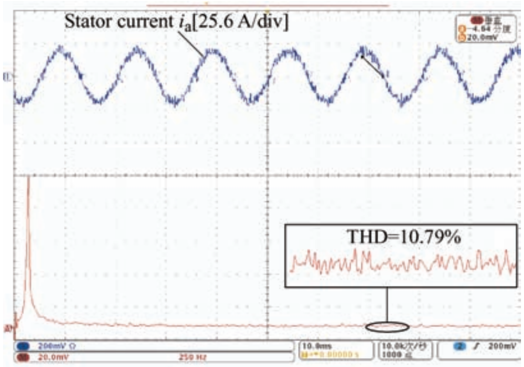

(a) i_a experimental waveform and its FFT analysis under the conventional MPCC method

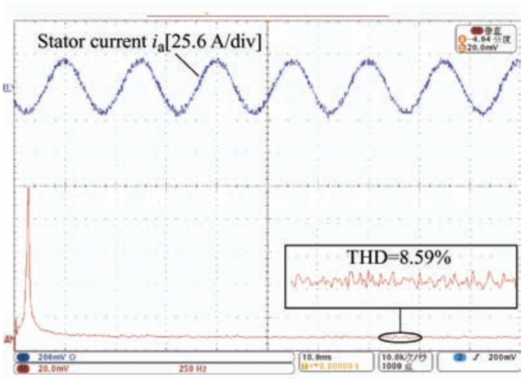

(b) i_a experimental waveform and its FFT analysis under the proposed MPCC method

Fig. 6 PMSM experimental waveform at rated speed and rated torque

To further compare the steady-state performance of the two control algorithms, the line graph of the pulsation value corresponding to each increase in the motor speed by 500 r/min is presented in Fig. 7. In the low-speed range (500-1 500 r/min), the current pulsation value of IOD-MPCC is lower than that of ODC-MPCC, whereas in the medium and high-speed range (2 000-3 000 r/min), the current pulsation value of IOD-MPCC exhibits a more significant reduction than that of ODC-MPCC. Therefore, the steady-state performance of IOD-MPCC is better than that of ODC-MPCC.

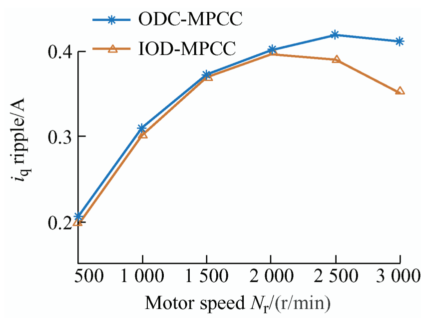

(a) i_q ripple value at different speeds

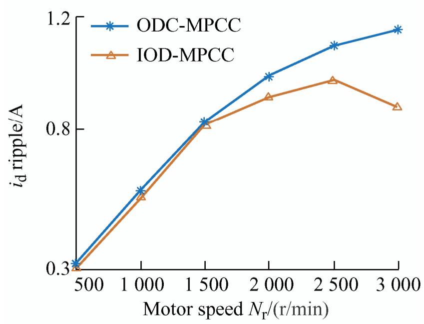

(b) i_d ripple value at different speeds

Fig. 7 Current ripple values of ODC-MPCC and IOD-MPCC at different speeds

The actual current ripple value obtained from the motor when it is running at a rated torque of 15 N·m and rated speed of 3 000 r/min is recorded in Tab. 3. The table shows that, compared with the ODC-MPCC strategy, the d-axis current ripple value of the IOD-MPCC strategy is reduced by approximately 23.5%, and the q-axis current ripple value is reduced by 14.74%. Experimental results show that IOD-MPCC can reduce stator current ripples.

Tab. 3 Current ripple values of the two control strategies at rated torque (15 N·m) **and speed** (3 000 r/min)

Control strategy	Δi_d/A	Δi_q/A
ODC-MPCC	1.152 9	0.412 4
IOD-MPCC	0.881 8	0.351 6

4.2 Dynamic analysis

(1) Experimental waveforms when the motor is under a variable torque.

At the beginning of the experiment, the motor was switched on without a load at a given speed of 3 000 r/min. The load torque abruptly increased to 10 N·m at 0.1 s and decreased to 5 N·m at 0.35 s.

The waveforms of the variable torque control experiment of PMSM under the ODC-MPCC method are presented in Figs. 8a and 8b. The waveforms of the variable torque control experiment of PMSM under the IOD-MPCC method are illustrated in Figs. 8c and 8d.

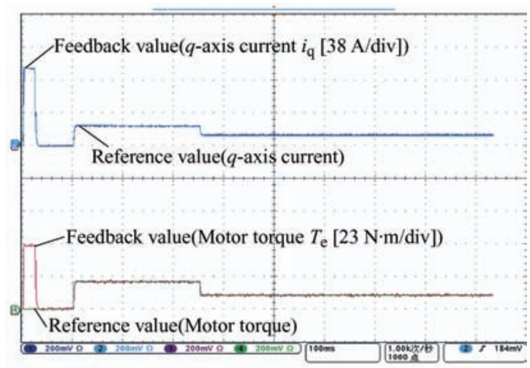

(a) q-axis current and motor torque waveforms under conventional MPCC method

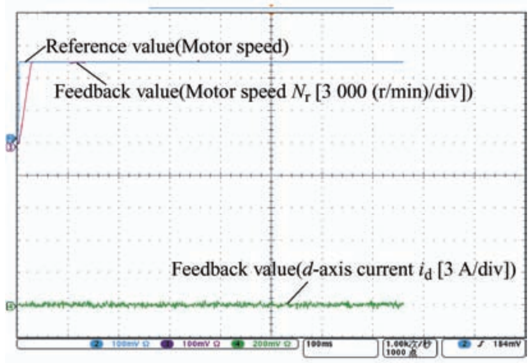

(b) Motor speed and d-axis current waveforms under conventional MPCC method

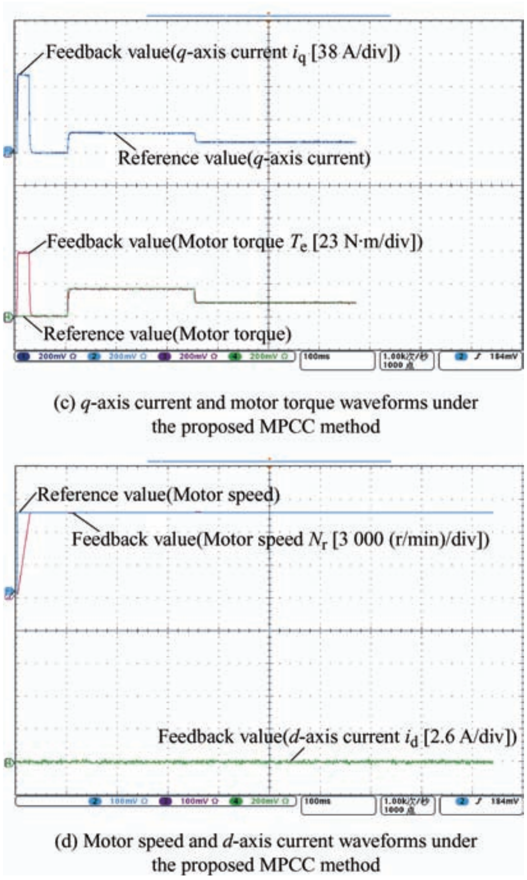

(c) *q*-axis current and motor torque waveforms under the proposed MPCC method

(d) Motor speed and *d*-axis current waveforms under the proposed MPCC method

Fig. 8 Response to variation in torque reference under the two methods

Fig. 8 clearly demonstrates that the ODC-MPCC and IOD-MPCC current pulsations are equivalent, and the current tracking performance is optimal. After the PMSM torque is altered abruptly, IOD-MPCC still exhibits the same rapid torque response as ODC-MPCC (the response time is approximately 0.008 s). Under the two control strategies, the speed of the motor has a certain drop; however, they can quickly track the specified reference command after 0.04 s, such that their anti-disturbance ability is similar.

(2) Experimental waveforms when the motor is under variable speed.

At the beginning of the experiment, the motor was switched on at a speed of 1 500 r/min and rated torque of 15 N·m at 0.15 s. At 0.35 s, the motor speed was reduced to 500 r/min and then increased to 1 000 r/ min at 0.45 s.

The waveforms of the variable speed control experiment of PMSM under the ODC-MPCC method are presented in Figs. 9a and 9b. The waveforms of the variable speed control experiment of PMSM under the IOD-MPCC method are presented in Figs. 9c and 9d.

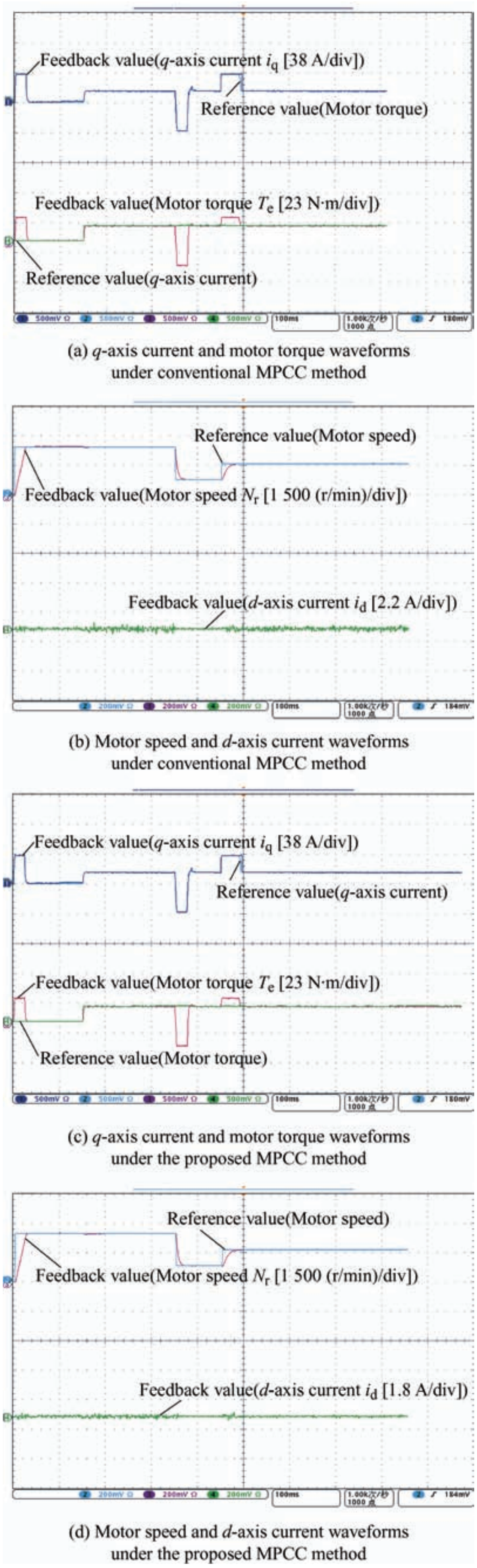

(a) *q*-axis current and motor torque waveforms under conventional MPCC method

(b) Motor speed and *d*-axis current waveforms under conventional MPCC method

(c) *q*-axis current and motor torque waveforms under the proposed MPCC method

(d) Motor speed and *d*-axis current waveforms under the proposed MPCC method

Fig. 9 Response to variation of speed reference under the two methods

By analyzing Fig. 9, we can observe that the ODC-MPCC and IOD-MPCC current pulsations are equivalent, and the current tracking performance is optimal. After the PMSM speed is abruptly altered, IOD-MPCC still exhibits the same rapid speed response as ODC-MPCC (the response time is approximately 0.025 s). Under the two control strategies, the torque of the motor exhibits a certain drop; however, the specified reference command after 0.09 s can be quickly tracked, such that their anti-disturbance ability is similar.

Accordingly, IOD-MPCC exhibited a better steady-state performance than ODC-MPCC. The reduction in the d-axis current ripple value is more significant than the reduction in the q-axis current ripple value. This result was obtained because IOD-MPCC is not limited to the zero voltage vector when selecting the second voltage vector, and it expands the selection range of the voltage vector. Furthermore, the experimental results of the variable torque and speed controls indicate that ODC-MPCC exhibits a dynamic response speed equivalent to that of IOD-MPCC, and their dynamic performance is equivalent. In terms of the number of current predictions, IOD-MPCC reduces the computational burden of ODC-MPCC.

5 Conclusions

To address the poor steady-state performance and large calculation burden of the conventional dual-vector MPCC, an improved optimal duty cycle MPC strategy is proposed. The proposed algorithm limits the number of candidate voltage vectors at the next moment to three, and the combination of voltage vectors to five. Finally, via experimental verification, the following conclusions are drawn.

(1) Compared with the conventual method, the THD value of the stator phase current is reduced by 20%, and the steady-state performance is improved.

(2) Under the rated speed and rated torque, the d- and q-axis current ripple values are reduced by approximately 23.5% and 14.74%, respectively. In addition, the stator current ripple is reduced.

(3) The computational burden of the proposed algorithm did not increase, and a dynamic performance comparable with the conventional algorithm was obtained.

References

[1] F Wang, L He, J Rodriguez. FPGA-based continuous control set model predictive current control for PMSM system using multistep error tracking technique. *IEEE Transactions on Power Electronics*, 2020, 35(12): 13455-13464.

[2] M S R Saeed, W Song, B Yu, et al. Low-complexity deadbeat model predictive current control with duty ratio for five-phase PMSM drives. *IEEE Transactions on Power Electronics*, 2020, 35(11): 12085-12099.

[3] J Gao, C Gong, W Li, et al. Novel compensation strategy for calculation delay of finite control set model predictive current control in PMSM. *IEEE Transactions on Industrial Electronics*, 2020, 67(7): 5816-5819.

[4] M Siami, D A Khaburi, A Abbaszadeh, et al. Robustness improvement of predictive current control using on prediction error correction for permanent magnet synchronous machines. *IEEE Access*, 2019, 7: 45898-45910.

[5] C Jia, X Wang, Y Liang, et al. Robust current controller for IPMSM drives based on explicit model predictive control with online disturbance observer. *IEEE Transactions on Industrial Electronics*, 2016, 63(6): 3458-3466.

[6] Z Chen, J Qiu，M Jin. Prediction-error-driven position estimation method for finite-control-set model predictive control of interior permanent magnet synchronous motors. *IEEE Journal of Emerging and Selected Topics in Power Electronics*, 2019, 7(1): 282-295.

[7] K Shen, J Feng, J Zhang. Finite control set model predictive control with feedback correction for power converters. *CES Transactions on Electrical Machines and Systems*, 2018, 2(3): 312-319.

[8] Zhan S, Yan S, Wei C, et al. Predictive duty cycle control of three-phase active-frontend rectifiers. *IEEE Transactions on Power Electronics*, 2016, 31(1): 698-710.

[9] X Li, P Shamsi. Model predictive current control of switched reluctance motors with inductance auto-calibration. *IEEE Transactions on Industrial Electronics*, 2016, 63(6): 3934-3941.

[10] Y Zhang, D Xu, J Liu. Performance improvement of model-predictive current control of permanent magnet synchronous motor drives. *IEEE Transactions on Industry Applications*, 2017, 53(4): 3683-3695.

[11] A M Bozorgi, M Farasat, S Jafarishiadeh. Model predictive current control of surface-mounted permanent magnet synchronous motor with low torque and current ripple. *IET Power Electronics*, 2017, 10(10): 1120-1128.

[12] Y Zhang, H Yang. Two-vector-based model predictive torque control without weighting factors for induction motor drives. *IEEE Transactions on Power Electronics*, 2015, 31(2): 1381-1390.

[13] Y Xu, B Zhang, Q Zhou. Two-vector based model predictive current control for permanent magnet synchronous motor. *Transactions of China Electrotechnical Society*, 2017, 32(20): 222-230.

[14] T Shi, W Zhang, Meng X, et al. Predictive current control for permanent magnet synchronous motor based on operating time of vector. *Transactions of China Electrotechnical Society*, 2017, 32(19): 1-10.

[15] Y Yan, S Wang, C Xia, et al. Hybrid control set-model predictive control for field-oriented control of VSI-PMSM. *IEEE Transactions on Energy Conversion*, 2016, 31(4): 1622-1633.

[16] Z Lan, B Wang, C Xu, et al. A novel three-vector model predictive current control for permanent magnet synchronous motor. *Proceedings of the CSEE*, 2018, 38(S1): 243-249.

[17] Y Xu, B Zhang, Q Zhou, et al. Optimal duty cycle model predictive current control based on SVM. *Electric Drive,* 2017, 47(7): 12-16.

Dingdou Wen received the B.S. degree in Automation from Nanjing Tech. University, Nanjing, China, in 1993, the M.S. degree in Control Theory and Control Engineering from Central South University, Changsha, in 2007. He has been with Hunan University of Technology, he is currently a Professor of Automatic Control Engineering. His current research interests are permanent magnet synchronous motor speed control.

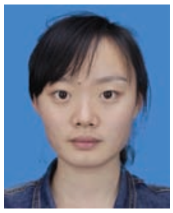

Jie Yuan, master's degree student of Hunan University of Technology, mainly researching power electronics and electric drive.

Yang Zhang received his B.S. degree in Applied Physics and his M.S. degree in Electrical Engineering from Hunan University of Technology, Zhuzhou, China. He received his Ph.D. degree in Electrical Engineering from Hunan University, Hunan, China, in 2017.

He is currently an Assistant Professor in Hunan University of Technology. His current research interests include wind power generation system and impedance-source converters.

Chuandong Shi, master's degree student of Hunan University of Technology, mainly researching power electronics and electric drive.